Structural and Conformational Requirements for High-Affinity Binding to the SH2 Domain of Grb2[1]

Peter Ettmayer,*,† Dennis France,‡,|| John Gounarides,‡,§ Mark Jarosinski,||,⊥ Mary-Sue Martin,‡,|| Jean-Michel Rondeau,▽ Michael Sabio,‡,§ Sid Topiol,‡,§ Beat Weidmann,‡,|| Mauro Zurini,▽ and Kenneth W. Bair‡,||

Novartis Forschungsinstitut, Brunnerstrasse 59, Vienna A-1235, Austria, Novartis Institute for Biomedical Research, Novartis Pharmaceuticals Corp., Summit, New Jersey 07901, and Novartis Pharma AG, CH-4002 Basel, Switzerland

Received October 5, 1998

Following earlier work on cystine-bridged peptides, cyclic phosphopeptides containing nonreducible mimics of cystine were synthesized that show high affinity and specificity toward the Src homology (SH2) domain of the growth factor receptor-binding protein (Grb2). Replacement of the cystine in the cyclic heptapeptide cyclo(CY*VNVPC) by D-α-acetylthialysine or D-α-lysine gave cyclo(Y*VNVP(D-α-acetyl-thiaK)) (**22**) and cyclo(Y*VNVP(D-α-acetyl-K)) (**30**), which showed improved binding 10-fold relative to that of the control peptide KPFY*VNVEF (**1**). NMR spectroscopy and molecular modeling experiments indicate that a β-turn conformation centered around Y*VNV is essential for high-affinity binding. X-ray structure analyses show that the linear peptide **1** and the cyclic compound **21** adopt a similar binding mode with a β-turn conformation. Our data confirm the unique structural requirements of the ligand binding site of the SH2 domain of Grb2. Moreover, the potency of our cyclic lactams can be explained by the stabilization of the β-turn conformation by three intramolecular hydrogen bonds (one mediated by an H_2O molecule). These stable and easily accessible cyclic peptides can serve as templates for the evaluation of phosphotyrosine surrogates and further chemical elaboration.

Introduction

The growth factor receptor-binding (Grb2) adaptor protein plays a central role in signaling by receptor tyrosine kinases. Grb2 is necessary for activation of the Ras pathway via complex formation with the Ras exchange factor Sos.[2] The Src homology (SH2) domain of Grb2 binds preferentially to phosphotyrosines (Y*s) with the sequence motif Y*XNX. The two SH3 domains of Grb2 bind to Sos, which catalyzes GTP/GDP exchange on Ras, thereby activating the GTPase and downstream kinase cascade. Compounds which selectively antagonize the SH2 domain of Grb2 should interrupt these signaling pathways and are thus attractive targets for drug therapy in oncology.[3]

We started our research on low-molecular weight Grb-SH2 antagonists looking for phosphopetides with high affinity toward the adaptor protein. Systematic alanine and cysteine scans of the nonapeptide EPQY*VNVPI led to the discovery of both linear and cyclic peptides with up to 35 times higher binding affinity than the control peptide KPFY*VNVEF (**1**, amino acid residues 174−182 of Bcr-Abl[3,4]) in a competitive ELISA.[5] All these compounds featured the Y*VNV sequence and C- and N-terminal cysteines. To further assess the value of cyclic peptides for Grb2-SH2 antagonism, we investigated the conformation of the cyclic phosphopeptide **2** (cyclo(CY*VNVPC)) bound to Grb2-SH2. The X-ray-derived coordinates of the SH2 domain of the adaptor protein bound to the linear peptide **1** served as the starting point for molecular dynamics and molecular mechanics geometry optimizations.

We first synthesized cyclic lactams using cystine surrogates to close the ring. Structure−activity data, together with the modeling studies and protein crystallography, allowed us to identify the origin of the potency of these cyclic peptides. The identification of these novel, more stable cyclic compounds provides a starting point for the creation of improved, less peptidic Grb2-SH2 antagonists.

Results and Discussion

Models of Cyclic Phosphopeptide CY*VNVPC (2) Bound to the Grb2-SH2 Domain. To obtain the coordinates of a Grb2-SH2 domain/ligand complex for subsequent molecular modeling studies, we determined the X-ray structure of Grb2-SH2 bound to the linear peptide KPFY*VNVEF (**1**) at 1.80-Å resolution (Figure 1). The peptide was found to adopt a compact, folded conformation, characterized by a regular type I β-turn for the core residue Y*VNV. This result is in full agreement with the recently published crystal structure of the complex with the shorter peptide KPFY*VNV[6] and with an NMR-derived solution structure of a Shc peptide bound to Grb2-SH2.[7] This bent conformation is in marked contrast to the extended binding mode observed for all other SH2 domains examined to date.[8] The classical +3 pocket which is found in other SH2 domains is sterically blocked in Grb2-SH2 by the bulky side chains of Trp121 and Arg142. Trp121 has been identified as a major determinant of the unique specificity of Grb2-SH2,[9] which exclusively selects Asn at position +2.[10,11] In the X-ray structure, this residue is

* To whom correspondence should be addressed. Phone: +43 1 866 34-9038. Fax: +43 1 866 34-582. E-mail: peter.ettmayer@pharma.novartis.com.
† Novartis Forschungsinstitut.
‡ Novartis Institute for Biomedical Research (NIBR).
§ Core Technology Area, NIBR.
|| Oncology Therapeutic Area, NIBR
⊥ Present address: Amgen Inc., Boulder, CO 80301.
▽ Novartis Pharma AG.

10.1021/jm9811007 CCC: $18.00
Published on Web 03/02/1999

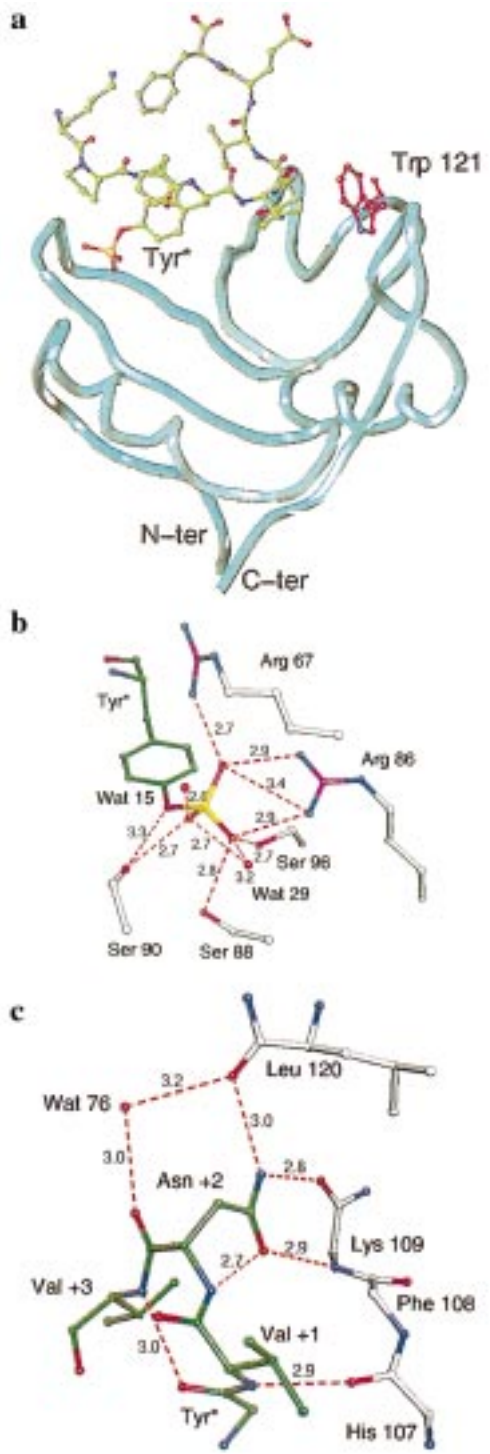

Figure 1. X-ray structure of the SH2 domain of Grb2 in complex with **1**. (a) Overall view of the complex. The ligand is shown in ball-and-stick representation, and the fold of the polypeptide chain of the SH2 domain is depicted as a tube. The side chain of Trp121 is shown in red. This amino acid residue forces the ligand into a turn conformation. (b) Closeup of the phosphotyrosine binding pocket. For clarity, only residues which are hydrogen-bonded to the phosphate moiety of Y* are shown. (c) Hydrogen-bonded interactions between Val+1, Asn+2, and the SH2 domain. For clarity, only main-chain atoms are shown for the protein.

packed against the indole moiety of Trp121, and its side-chain amide group is involved in one hydrogen bond with the backbone nitrogen atom of Lys109 and two hydrogen bonds with the backbone oxygen atoms of Lys109 and Leu120. The Y* makes extensive interactions with the SH2 domain, which are very similar to the ones seen in other SH2 domain/ligand complexes.[7] In contrast, Lys-3, Pro-2, Val+3, Glu+4, and Phe+5 of the peptide make little or no contact with the SH2 domain. Therefore, and in agreement with the known substrate specificity of Grb2-SH2, binding affinity is primarily driven by the Y*, while specificity appears to be dictated by the unique β-turn conformation and the interactions mediated by Asn+2.[12]

On the basis of this experimental structure, models of the Grb2-SH2/**2** complex were developed. The coordinates of the Y*VNV fragment of **1** in the X-ray structure were used to build a model of **2** with inter- and intramolecular distance range constraints based on the described[6,13] interactions of Asn+2 and Y* with the Grb2-SH2 domain and the presence of a type-1 β-turn in the ligand. All atoms of the protein were fixed, and a molecular mechanics optimization including electrostatics was performed with the ligand allowed to relax under the influence of the range constraints. The energy-minimized model was submitted to a molecular dynamics simulation at 900 K. A total of 100 structures were extracted at 500-fs intervals from the dynamics trajectory and were optimized with the same fixed atom set and range constraints as used for the first geometric relaxation of the docked ligand. The resulting 100 low-energy conformers of **2** were clustered into 10 sets based on identical hydrogen-bonding patterns (Table 1). All conformers showed the intermolecular hydrogen bond observed in the crystal structure between Val+1 and His107. In addition to having this common feature, these conformations are characterized by competition between the carbonyl group of Cys-1 (sets **4**−**10**) and the carboxyl group of Cys+5 for the interaction with Arg67 (highly conserved in SH2 domains[14]) and Arg142 (sets **1**−**3**). No conformation was found that had a pronounced interaction between the carbonyl group of the *N*-acetyl group in the cyclic phosphopeptide **2** and the Grb2-SH2 domain.[15]

Though this limited[16] computational model provided an approach for understanding the specificity of cyclic peptides toward Grb2-SH2, we were not able to select one of the 10 clusters as being representative of the most likely binding mode for the cyclic peptide in complex with the Grb2-SH2 domain. To further assess which intra- and intermolecular hydrogen bonds contribute most to high-affinity binding in these Grb2-SH2 antagonists, we started a medicinal chemistry program. Rationally designed compounds of various ring size, lacking the *N*-acetyl of Cys-1 and/or the carboxy group of Cys+5, should help to identify the source of high-affinity binding.

Synthesis of Cyclic Phosphopeptides. The non-cystine-bridged peptides and carbamates were synthesized as outlined in Scheme 1. The linear peptide **3** incorporating an *O*-2,6-dichlorobenzyl-protected tyrosine was first assembled on solid phase using acid-labile Wang resin and diisopropylcarbodiimide (DIC) in the presence of 1 equiv of 1-hydroxybenzotriazole (HOBt). Because of the C-terminal proline, it was necessary to couple the next two amino acids (Val, Asn) as a dipeptide (Asn-Val).[17] Stepwise coupling of the Fmoc-

Table 1. Observed Inter- and Intramolecular Hydrogen Bonds[a] in the Low-Energy Conformers of **2** Bound to Grb2-SH2

	intermolecular			intramolecular						
set	C-1 → Arg67	C+5 → Arg142	H107 → V+1	Y* → V+3	Y* → N+2	V+3 → Y*	V+3 → C+5	N+2 → V+3	C+5 →	V+1 → C+5
1	−	+	+	+	−	−	−	−	−	+
2	−	++	+	+	+	−	−	+	−	−
3	−	+	+	+	−	−	−	−	−	−
4	++	−	+	+	−	−	+	−	Y*, C-1, C-1	−
5	++	−	+	−	−	−	−	+	−	−
6	++	−	+	−	−	−	−	−	−	−
7	++	−	+	−	−	+	−	−	−	−
8	++	−	+	+	−	+	−	−	−	−
9	++	−	+	+	−	+	−	−	−	−
10	+	−	+	+	−	+	−	−	−	−

[a] The number of hydrogen bonds is equal to the number of "+" symbols; syntax: C=O → H−N. All compounds have hydrogen bonds between the $CONH_2$ of N+2 and LYS109 and LEU120. No hydrogen bonds were found between the *N*-acetyl group in **2** and Arg67.

Scheme 1[a]

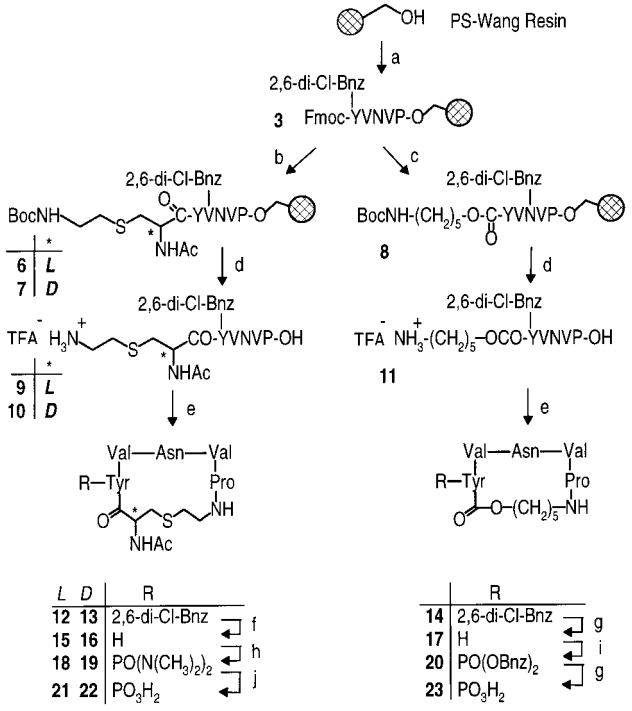

[a] Conditions: (a) Fmoc deprotection with 20% piperidine in DMF, coupling of Fmoc-NV, Fmoc-V, Fmoc-(2,6-di-Cl-Bnz)Y, DIC, HOBt, DMF, 5−12 h, rt; (b) 20% piperidine in DMF, then (*R*)- or (*S*)-*N*-acetyl-*S*-(2-aminoethyl)cysteine (**4, 5**), DIC, HOBt; (c) 20% piperidine in DMF, then BocNH-$(CH_2)_5$-OH, phosgene, pyridine, CH_2Cl_2; (d) 5% H_2O and 3% Et_3SiH in TFA, 2 h, rt; (e) DPPA, DIEA, 0.002 M in DMF, 72 h, rt; (f) 10% Pd/C, H_2, 10% HCOOH/EtOH, 12 h, 70 °C; (g) 10% Pd/C, H_2, EtOH, 12 h, rt; (h) $POCl(N(CH_3)_2)$, DBU, DMAP, CH_2Cl_2, 2 h, 0 °C to rt; (i) first $P(OBnz)_2N(isopropyl)_2$, tetrazole, THF, 0 °C, then $(CH_3)_3COOH$; (j) 2 N HCl, 12 h, rt.

protected amino acids was unsuccessful due to diketopiperazine formation.

Coupling **3** with Boc-protected amino acids **4** and **5** using DIC/HOBt afforded the linear peptides **6** and **7**). Reacting deprotected **3** with Boc-protected 5-aminohexanol in the presence of phosgene and a base gave the carbamate **8**. Simultaneous removal of the Boc protecting group and cleavage from the resin (TFA/H_2O/$HSiEt_3$) gave the acids **9**−**11** in quantitative yields and high purity (>95% by RP-HPLC). No additional chromatographic purification was necessary. Macrocyclization was carried out using diphenylphosphoryl azide (DPPA) and diisopropylethylamine (DIEA) in DMF (0.0013 M) affording **12**−**14** in ∼60% yield. The *O*-(2,6-dichlorobenzyl)tyrosine protecting group was removed by catalytic hydrogenation (10% Pd/C) to give the unprotected cyclic peptides **15** and **16** and the cyclic carbamate **17**.

15 and **16** were treated with tetramethylphosphorodiamidic chloride and 4-(dimethylamino)pyridine/1,8-diazabicyclo[5.4.0]undec-7-ene (DMAP/DBU) in CH_2Cl_2/DMF to yield the Y* derivatives **18** and **19** in ∼50% purified yield. By introducing a P^V (instead of a P^{III}) atom directly, this method avoids the oxidation step which would not be compatible with the sulfur-containing peptides. The cyclic phosphocarbamate **20** was produced by treatment of **17** with dibenzyl isopropylphosphoramidite and tetrazole in THF followed by oxidation with *tert*-butyl hydroperoxide. Hydrolysis of **18** and **19** in 1 N HCl overnight followed by RP-HPLC purification gave the free Y*-containing cyclic peptides **21** and **22**. Catalytic hydrogenation of **20** gave **23** in quantitative yields and high purity. The cyclic phosphopeptides **25**−**33** were synthesized using the phosphoramidite/tetrazole procedure described for compound **23**.

The linear peptides **1** and **24** and the precursor of the cyclic peptide **2** were assembled on solid phase using Fmoc chemistry and Fmoc-Tyr[$PO((NCH_3)_2)_2$]-OH[18] for the phosphotyrosine residue. Simultaneous deprotection and cleavage from the resin was followed by RP-HPLC purification. The cyclic peptide **2** was obtained in 80% yield after oxidation with 20% v/v aqueous DMSO in the presence of Ekathiox resin.

Structure−Activity Relationships. Inhibition of binding of Grb2-SH2 to biotinylated KPFY*VNVEF was measured using a competitive ELISA. As a specificity control, inhibition of binding of biotinylated EPQY*EEIPI to Src-SH2 was determined. IC_{50} values were adjusted to match a common value for the control peptide (**1** (KPFY*VNVEF), IC_{50}(Grb2-SH2) = 0.7 μM; **24** (EPQY*-EEIPI), IC_{50}(Src-SH2) = 6.3 μM) which was included in each plate (see Experimental Section for details).

The cyclic phospholactam **25** and the linear phosphopeptide **26** were first synthesized to mimic the oxidized and reduced forms of the cystine-containing lead compound **2**. **25** has the same ring size as **2** but does not have the N-terminal acetyl group and the C-terminal carboxylate moiety. **26** is a mimic of the reduced, linear form of **2** but cannot cyclize under assay conditions. **25** was 3-fold more active than the linear compound **26** but

Table 2. Relative Binding Affinities (IC_{50}) of Cyclic Phosphopeptides for Grb2-SH2 and Src-SH2:[a] Variation in Ring Size and Type

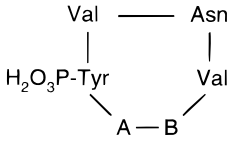

			IC_{50} (μM)	
compd	A	B	Grb2-SH2[b]	Src-SH2[c]
2	L-(α-acetyl-Cys-SS-Cys)	L-Pro	0.06 ± 0.03 (5)	38
25	7-aminoheptanoyl	L-Pro	0.60 ± 0.16 (6)	>100
26	*d*		1.63 ± 0.40 (6)	>100
27	glycyl	L-Pro	0.52 ± 0.20 (2)	>100
28	glycyl	D-Pro	10.83 ± 7.31 (2)	>100
23	−CO−O−$(CH_2)_5$−NH−	L-Pro	0.71 ± 0.19 (6)	>100
29	L-α-acetyllysyl	L-Pro	0.18 ± 0.05 (5)	73
30	D-α-acetyllysyl	L-Pro	0.07 ± 0.03 (3)	>150
21	L-α-acetylthialysyl	L-Pro	0.11 ± 0.03 (7)	88
22	D-α-acetylthialysyl	L-Pro	0.06 ± 0.03 (7)	55

[a] Reported are the concentrations at which half-maximal inhibition (IC_{50}) of binding of Grb2-SH2 to biotinylated KPFY*VNVEF and inhibition of binding of biotinylated EPQY*EEIPI to Src-SH2 was observed. IC_{50} of control peptide KPFY*VNVEF (**1**): 0.7 ± 0.14 μM. [b] Mean value with standard deviation, number of determinations in parentheses. [c] IC_{50} of control peptide EPQY*EEIPI (**24**): 6.3 ± 0.9 μM. [d] CH_3−CH_2−CO−(phospho)Tyr-Val-Asn-Val-Pro-NH-Bu.

Table 3. Relative Binding Affinities (IC_{50}) of Cyclic Phosphopeptides for Grb2-SH2 and Src-SH2:[a] Variation in X+1 and X+3

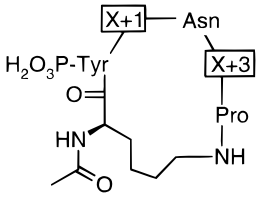

			IC_{50} (μM)	
compd	X+1	X+3	Grb2-SH2[b]	Src-SH2[c]
30	Val	Val	0.07 ± 0.03 (3)	>150
31	Leu	Val	1.34 ± 0.33 (3)	>150
32	Cha	Val	1.61 ± 0.11 (3)	>150
33	Val	Cha	0.11 ± 0.02 (3)	>150

[a] Reported are the concentrations at which half-maximal inhibition (IC_{50}) of binding of Grb2-SH2 to biotinylated KPFY*VNVEF and inhibition of binding of biotinylated EPQY*EEIPI to Src-SH2 was observed. IC_{50} of control peptide KPFY*VNVEF (**1**): 0.7 ± 0.14 μM. [b] Mean value with standard deviation, number of determinations in parentheses. [c] IC_{50} of control peptide EPQY*EEIPI (**24**): 6.3 ± 0.9 μM.

less active than the lead compound **2** by a factor of ∼10 (Table 2). Since these effects may arise from conformational differences in the critical recognition motif Y*VNV of **2, 25**, and **26**, we used NMR spectroscopy to determine the conformations of the peptides in aqueous solution (Table 4, see the Experimental Section).

A strong $N+2_{NH}$−$V+3_{NH}$ ROE, a weak $N+2_{\alpha CH}$−$V+3_{NH}$ ROE, and a nonsequential $V+1_{\alpha CH}$−$V+3_{NH}$ ROE are observed for cyclic structures **2** and **25**. These ROEs, as well as the small $^3J_{N\alpha}$ coupling constant of V+1 (**2**, 4.5 Hz; **25**, 4.4 Hz), indicate that the Y*VNV motif in **2** and **26** adopts highly populated β-turn conformations.[19] In **2** and **25** the chemical shift temperature coefficient (NH $d\delta/dT$) of the $V+3_{NH}$ (**2**, −2.8 ppb/K; **25**, −3.3 ppb/K) is consistent with intramolecular hydrogen bonding, presumably to the Y* carbonyl, as expected for these β-turns conformations. In addition to the above ROEs, **2** and **25** exhibit very strong $V+1_{\alpha CH}$−$N+2_{NH}$ and $N+2_{\alpha CH}$−$N+2_{NH}$ ROEs, which are consistent with a type II β-turn, as well as a weak $V+1_{NH}$−$N+2_{NH}$ ROE, suggesting the presence of a type I β-turn conformation. Therefore, the Y*VNV sequence in **2** and **26** may adopt both β-turn configurations. In contrast, the $^3J_{N\alpha}$ coupling constant, temperature coefficent, and ROE data (see Table 4) for the linear peptide **26** do not indicate the presence of a preferred conformation in solution. From this NMR data, we concluded that, in aqueous solution, the Y*VNV motif forms a virtually identical type I/type II β-turn in both cyclic phosphopeptides **2** and **25**, while it is a random coil in the linear peptide **26**.

Having thus established the predominance of the cyclic structure in solution, we synthesized a variety of cyclic structures. The cyclic derivative **23** was obtained by replacement of the cystine moiety with 5-aminopentanol and attachment of the hydroxyl group to the Y* via a carbamate linkage. This compound has the same number of backbone atoms as **25** and also the same binding affinity. Replacing the α-acetylcysteine in **2** by glycine gave **27**, the smallest hexapeptide possible that still contains the Y*VNVP sequence. In aqueous solution the Y*VNV sequence of **27** favors the type I β-turn configuration, as judged by the strong $V+1_{NH}$−$N+2_{NH}$ ROE, the weak $V+1_{\alpha CH}$−$N+2_{NH}$ ROE, and the weak $N+2_{\alpha CH}$−$N+2_{NH}$ ROE. These ROEs can be compared to the corresponding ROEs in **2** and **25** (see Table 4). In addition **27** adopts a type II β-turn conformation centered on Pro-Gly (data not shown). While the type I β-turn is favored in **27,** this compound was only marginally better than the 7-aminoheptanoyl derivative **25** and still significantly less active than the lead compound **2**. Hence, stabilizing a type I β-turn for the Y*VNV motif does not ensure improved binding affinity. Replacement of the Pro by D-Pro (**27** → **28**) produced a 100-fold decrease in binding affinity, indicating unfavorable interactions between the resulting compound and the SH2 domain.

Substitution of the *N*-acetyl cystine in **2** by L- or D-*N*-α-acetyllysine gave the cyclic peptides **29** and **30**. This substitution in effect removes the carboxylic acid moiety and reduces the size of the ring by one atom. Both *N*-α-acetyllysine derivatives were more potent than the 7-aminoheptanoyl (**25**) and (**27**) glycyl derivatives, with

Table 4. Significant Chemical Shifts (δ, ppm), Coupling Constants (J, Hz), Temperature Coefficients (δ/T, ppb/K), and Observed ROEs for Compounds **2**, **25**, **26**, **22**, and **27** in Aqueous Solution at pH 2.8−3.3, 293 K

		Y*			V+1			N+2			V+3		
compd	T (K)	δ(NH)	$^3J_{N\alpha}$	NH dδ/dT	δ(NH)	$^3J_{N\alpha}$	NH dδ/dT	δ(NH)	$^3J_{N\alpha}$	NH dδ/dT	δ(NH)	$^3J_{N\alpha}$	NH dδ/dT
2	293	8.58	7.7	−13	8.14	4.5	−10	8.52	7.4	−8.4	7.67	9.1	−2.8
25	293	7.91	7.8	−7.1	8.04	4.4	−9.3	8.54	7.5	−7.6	7.70	9.2	−3.3
26	293	8.15	7.0	−9.2	8.06	8.2	−6.8	8.51	7.2	−7.7	8.17	8.0	−11.0
27	293	8.66	9.2	−2.9	8.13	6.1	−9.0	8.79	8.7	−6.9	7.37	7.9	−1.0
22	293	8.23	8.6	−5.0	8.65	2.9	−8.8	8.68	7.2	−7.6	7.72	8.5	−3.2

compd	V+1$_{\alpha CH}$−N+2$_{NH}$	V+1$_{NH}$−N+2$_{NH}$	V+1$_{\alpha CH}$−V+3$_{NH}$	N+2$_{\alpha CH}$−N+2$_{NH}$	N+2$_{\alpha CH}$−V+3$_{NH}$	N+2$_{NH}$−V+3$_{NH}$
2	VS[a]	VW	VW	S	W	S
25	VS	VW	VW	S	W	S
26	S			W	S	
27	W	S		W		S
22	S	*b*		M		S

[a] VW, very weak; W, weak; M, medium; S, strong; VS, very strong. [b] Not observed, presumably due to spectral overlap.

the D-compound (**30**) showing the best (10-fold) improvement in binding affinity. This result suggests that the *N*-acetyl group may be important. In contrast, the reintroduction of a sulfur atom in the *N*-α-acetyllysine linker (**21** and **22**) did not change the IC_{50} to a significant extent, while showing the same preference for D- over L-stereochemistry.

Within experimental error, the D-*N*-α-acetyllysyl and thialysyl derivatives were as potent as **2**. The ^{1}H NMR of **22** in aqueous solution is similar to that of **2** (Table 4).

Having established that *N*-acetylcystine in **2** can be replaced by D-*N*-α-acetyl lysine without sacrificing binding affinity to Grb2-SH2, we began to evaluate the contributions of Val+1 and Val+3 to the binding. Replacing Val+1 in **30** by leucine (**31**) or cyclohexylalanine (Cha; **32**) resulted in a 15- and 25-fold reduction in affinity, respectively, while the same replacements at Val+3 had almost no effect (Table 3). These data are consistent with the observation (Figure 1) that Val+1 is tightly bound while Val+3 makes only loose surface contacts with the Grb2-SH2 domain, with the recently published data on the binding of alanine-substituted Shc peptides to Grb2-SH2,[20] and with the SAR data on potent Grb2-SH2 antagonists.[21]

To assess specificity, the binding of all compounds to the Src-SH2 domain was also examined by ELISA. As expected, IC_{50} values were higher by at least 2 orders of magnitude in comparison to Grb2-SH2 (Table 2).[22] All intermediates (tyrosine and protected Y*-containing peptides) were also tested against Grb2-SH2. None was found active up to a concentration of 100 μM, showing that Y* is an essential determinant for recognition and high-affinity binding.[12]

X-ray Structure Analyses of Cyclic Phosphopeptide 21 in Complex with Grb2-SH2. The SAR data for Grb2-SH2 binding of these cyclic phosphopeptides highlighted the importance of the *N*-acetyl group on the amino acid Cys-1 and demonstrated that the carboxy group of Cys+5 (**2**) is of less importance. In the computational models described above, no interaction between the *N*-acetyl group and the protein was observed, suggesting that the *N*-acetyl group modulates cyclic peptide activity via an intramolecular interaction.

We were able to confirm this assumption with the X-ray structure of the Grb2-SH2/**21** complex which was determined at 2.10-Å resolution (Figure 2). This crystal structure shows that the key interactions made by the linear peptide KPFY*VNVEF (**1**) are maintained in the complex with the cyclic compound **21**. Notably, the β-turn conformation and the binding interactions made by the Y*VNV sequence are identical to those observed for the corresponding segment in the linear peptide (Figures 1 and 2). However, there are also a few interesting differences. While the intramolecular hydrogen bond between the carbonyl oxygen of Y* and the NH of Val+3 is conserved, there is now also a direct hydrogen bond between the NH of Y* and the carbonyl oxygen of Val+3, whereas this latter hydrogen bond was mediated by a bridging H_2O molecule in the complex with the linear peptide. In addition, a tighter interaction between the BC loop and the Y* of **21** is observed. In particular, the main-chain NH of Ser90 now makes a direct hydrogen bond to one of the phosphate oxygens, and the side chain of Glu89 folds over the Y* binding pocket, accepting a hydrogen bond from the protein main-chain NH of Arg67. These interactions were not observed in the complex with the linear peptide, presumably because of steric hindrance between Pro-2 of the ligand and Ser90 of the SH2 domain; it is also possible that crystal contacts favored a more open conformation of the BC loop in the complex with **1**, which crystallized in a different space group.

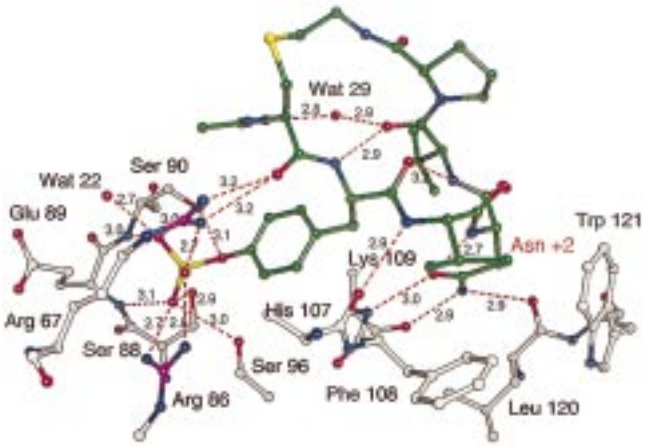

Figure 2. Intra- and intermolecular hydrogen-bonded interactions between **21** and the SH2 domain of Grb2. In addition to the binding interactions provided by the phosphate moiety of Y*, key hydrogen bonds are made by the Asn+2 side chain, the main-chain carbonyl oxygen of the residue at position −1, and the main-chain nitrogen of the residue at position +1. These hydrogen-bonded interactions are also observed in the complex with the linear peptide **1**.

The N-terminal acetyl group of the ligand, Val+3, Pro+4, and the linker region do not make any direct contact with the protein. The N-terminal acetyl group is in van der Waals contact with the side chain of Y*. It is also involved in an intramolecular hydrogen-bonded interaction with the carbonyl oxygen of Val+3, mediated by a bridging water molecule, and in this way may also contribute to the stabilization of the β-hairpin conformation and the resulting effect on SH2 domain binding. The observation that the lysyl and thialysyl derivatives display similar potencies can now be explained by the fact that the sulfur atom is not in contact with the protein.

Furthermore, because the β-turn conformation was maintained in the various peptides examined by NMR, we may conclude that the importance of the linker region for high-affinity binding comes from subtle effects on the conformation and dynamics of these cyclic molecules. The inter- and intramolecular hydrogen bonds observed for **21** bound to Grb2-SH2 in this experimentally determined structure match those found for set **9** (Table 1) in the dynamics simulation. We therefore can assume that set **9** reflects the binding conformation of **2** most closely. The role of the intramolecular hydrogen bonds is further highlighted by the fact that among all 10 conformer sets, sets **9** and **10** show the best fit with the conformation of **2** found in aqueous solution (data not shown).

Summary

Our objective was to identify the origin of the potent affinity of cystine-cyclized peptides incorporating the Y*VNV sequence toward the Grb2-SH2 domain, using a combination of classical medicinal chemistry approaches, molecular modeling, NMR, and protein crystallography techniques. While this work was in progress the X-ray structure of Grb2-SH2 in complex with KPFY*VNVNH$_2$ was published,[6] revealing a novel binding mode characterized by a β-turn conformation. Our X-ray data with the longer linear peptide KPFY*-VNVEF (**1**) confirm this finding and suggest that Grb2-SH2 recognizes a β-hairpin motif in its protein partners. In addition, we could demonstrate by NMR spectroscopy that the Y*VNV sequence in the unbound cyclic peptide CY*VNVPC (**2**) also adopts a β-turn conformation in solution. Systematic replacement of the cystine and determination of the solution conformation show that a β-turn conformation centered around Y*VNV is essential but may not be sufficient for high-affinity binding. The crystal structure of Grb2-SH2 complexed to the cyclic phosphopeptide **21** demonstrates that key interactions between the SH2 domain and the linear peptide are maintained in the complex with the cyclic analogue. Moreover, the potency of our cyclic lactams can be explained by the stabilization of the β-turn conformation by three intramolecular hydrogen bonds (one mediated by an H_2O molecule). This X-ray structure provides a sound basis for further chemical elaboration of these antagonists. Ongoing studies concentrate now on replacing the Y* with metabolically stable phosphonomethyl Phe derivatives.

Experimental Section

Expression of Recombinant Proteins used in the SH2 ELISA Assays. Full length Grb2 (residues 1−217) and the SH2 domain of Src (residues 60−152) were expressed as glutathione-*S*-transferase (GST) fusion proteins using the pGEX-2T expression vector system.[23] Expression of GST-Grb2 and GST-Src-SH2 by transformed *Escherichia coli* JBL21 was induced by addition of 1 mM isopropyl thiogalactoside to the culture media. *E. coli* were harvested by centrifugation and resuspended in PBS containing 1 mg/mL Pefabloc. *E. coli* were then lysed in a cell disruptor (Avestin) and centrifuged at 15000*g*. The recombinant proteins were purified from the supernatant by affinity chromatography on glutathione-sepharose beads (Pharmacia). GST-Grb2 or GST-Src was eluted from glutathione-sepharose with 50 mM reduced glutathione (pH 7.4), and the respective proteins were dialyzed against a buffer consisting of 50 mM Tris (pH 7.5), 150 mM NaCl, 1 mM EDTA, and 1 mM DTT. The proteins were then aliquoted and stored at −80 °C.

Grb2-SH2 Enzyme-Linked Immunosorbant Assay (ELISA). Reagents for the ELISAs for both Grb2 and Src were purchased from Sigma Chemical Co. unless otherwise stated. Nunc Immulon II ELISA plates were coated with 100 μL of a solution of 1.0 μg/mL streptavidin in Dulbecco's phosphate-buffered saline (PBS) and incubated overnight at 4 °C. ELISA plates were then washed three times with a buffer consisting of 50 mM Tris (pH 7.5), 0.15 M NaCl, and 0.05% Tween-20 (TBST). Nonspecific binding sites were blocked by the addition of 300 μL of Superblock (Pierce) and incubated for 1 h at room temperature). The blocking reagent was then removed and the plates were washed three times with TBST buffer and aspirated to dryness; 100 μL of a solution of the biotinylated phosphopeptide in ELISA assay buffer (EAB) (TBST buffer containing 0.25% bovine serum albumin and 1.0% sheep serum) was then added to each well. For the Grb2-SH2 ELISA, biotinylated KPFY*VNVEF was added at a final concentration of 4.0 nM, and for the Src-SH2 ELISA, biotinylated EPQY*EEPI was added at a final concentration of 6.0 nM. Control wells received 100 μL of EAB only. After 1 h at room temperature, the solution was removed and the plates were washed three times with TBST buffer. Compounds to be assayed were prepared as 5 mM stock solutions in PBS and diluted in EAB immediately prior to testing.

For the actual ELISAs, the test wells received 100 μL of EAB containing the test compounds at various concentrations and either GST-Grb2 or GST-Src at final concentrations of 4.0 or 6.0 nM in EAB. Control wells received GST-Grb2 or GST-Src in EAB only. KPFY*VNVEF (**1**) or EPQY*EEPI (**24**) was included on each plate as a positive control in their respective ELISAs. After 1 h at room temperature, the plates were washed three times with TBST and 100 μL of a 1:1000 dilution of a rabbit anti-GST antibody was added to each well. After an additional 1 h at room temperature, the plates were washed three times with TBST and 100 μL of a 1:1000 dilution of an alkaline-phosphatase conjugated goat anti-rabbit immunoglobulin antibody (Pierce) was added. After a final 1 h at room temperature, the plates were washed three times with TBST and developed by the addition of a 1.0 mg/mL solution of the colorimetric alkaline phosphatase substrate *p*-nitrophenyl phosphate in diethanolamine buffer. After 15 min, the plates were placed in a microplate spectrophotometer, and the absorbance of each well was determined at 405 nm when sextuplicate wells containing no inhibitor reached an OD (optical density) of 1.0−2.0. Under these conditions, the signal-to-noise ratio between wells with no inhibitors and wells receiving no biotinylated peptide averaged at least 15:1, and intra-assay coefficients of variation averaged below 3%. Wells which had received no biotinylated peptide were considered as background.

Percent inhibition was calculated using the following formula: percent inhibition = 100% − (absorbance in the presence of inhibitor − background)/(absorbance in the absence of inhibitor − background) × 100%. Dose−response relationships were constructed by nonlinear regression analysis of the competition curves, and 50% inhibitory (IC_{50}) concentrations were calculated from the regression lines.

Cloning and Expression of Recombinant Grb2 Protein for Structural Studies. Recombinant Grb2-SH2 was ex-

pressed in *E. coli* BL21(DE3)pLysS as inclusion bodies. The construct comprised residues 49−168 of the full length protein plus three additional amino acids at the N-terminus (MGS). After harvest, cells were lysed by sonication and the inclusion bodies isolated by conventional techniques. Refolding was done as follows*:* 5 g of crude inclusion bodies was dissolved in 40 mL of 20 mM *N*-(2-hydroxyethyl)piperazine-*N*′-2-ethanesulfonic acid (HEPES), pH 8.5, 100 mM NaCl, and 6 M guanidine•HCl. The solution was clarified by centrifugation and dialyzed overnight against 2 mL of 20 mM HEPES, pH 7.4, 100 mM NaCl, and 5 mM DTT. Precipitated protein was then removed by centrifugation and the clear supernatant applied to a 10-mL column of phosphotyrosine-sepharose 4B equilibrated in the same buffer. After baseline washing, bound protein was eluted with 100 mM phosphate buffer, pH 7.4. Purified Grb2-SH2 was further desalted on Sephadex G-25 coarse in 100 mM NaCl containing 0.02% NaN_3 and carefully concentrated to 15 mg/mL by ultrafiltration with an overall yield of about 50 mg. All steps were performed at 4 °C.

Crystallization. Grb2-SH2 was cocrystallized with the different peptides using the hanging drop method (2-fold molar excess of the ligand over protein from a 20 mg/mL aqueous stock solution added to the drop). Briefly, 5 μL of protein at 15 mg/mL in 100 mM NaCl, 0.02% NaN_3 was mixed with an equal volume of well solution and allowed to equilibrate against 1 mL of the latter at room temperature. Crystals appeared typically within 4−5 days. For peptide **1** (KPFY*-VNVEF) the best conditions were equilibration against 100 mM HEPES (pH 6.5) containing 46% of saturated $(NH_4)_2SO_4$ as precipitant, whereas for peptide **21** the optimal pH was around 7.0 and the $(NH_4)_2SO_4$ concentration 30%. The complex with **1** crystallized in space group $P4_12_12$ with unit cell dimensions of $a = b = 51.13$ Å, $c = 90.25$ Å and 1 complex per asymmetric unit (Matthews coefficient = 2.2 Å^3/Da). The complex with **21** crystallized in space group $P321$ with unit cell dimensions $a = b = 83.78$ Å, $c = 32.0$ Å, $\gamma = 120°$ and 1 complex per asymmetric unit (Matthews coefficient = 2.0 Å^3/Da).

X-ray Structure Determination. Grb2-SH2 complex with KPFY*VNVEF (1): Diffraction data were measured at room temperature with a DIP2020K dual image plate system (MAC Science). X-rays were generated by a FR591 rotating anode X-ray generator (Nonius) equipped with a 0.3-mm × 3.0-mm fine focus and a double mirror X-ray optical system. The generator was operated at 45 kV and 90 mA. A full data set was collected from one single crystal of approximate dimensions 0.3 mm × 0.3 mm × 1.0 mm at a crystal to detector distance of 60 mm. In total, 120 images were collected as 1.0° oscillation each using an exposure time of 600 s. The raw data were processed with Denzo and scaled with the program Scalepack.[24] A total of 143 688 observations were reduced to 11 700 unique reflections to 1.80-Å resolution ($R_{merge} = 0.074$, completeness = 99.7%). The structure was determined by molecular replacement with the program Amore,[25] using the coordinates of the SH2 domain of unliganded, full length Grb2 (PDB entry 1gri) as a search model. There was clear, unambiguous electron density for the ligand in the first electron density map. The structure was refined to 1.80-Å resolution with X-PLOR 3.1[26] using the Engh and Huber force field.[27] The final model has good geometry (rms bond distances = 0.007 Å, rms bond angles = 1.30°) and includes residues 56−153 of Grb2, residues 1−9 of the ligand, and 115 H_2O molecules. The final crystallographic *R*-factor for all data between 10.0 and 1.80-Å resolution is 0.186 ($R_{free} = 0.213$).

Grb2-SH2 complex with 21: Diffraction data were collected from one crystal at the ESRF (beamline BM1, $l = 0.873$ Å), with a MAR Research image plate system, and processed with Denzo.[24] The data set was 94.5% complete to 2.1-Å resolution ($R_{merge} = 0.044$, data redundancy = 4.6). The structure was solved by molecular replacement with the program AMORE.[25] The coordinates of the SH2 domain taken from the crystal structure of the complex with the linear peptide were used as a search model. The structure was refined at 2.10-Å resolution with X-PLOR 3.1[26] to a crystallographic *R*-factor of 0.195 ($R_{free} = 0.230$). The final model has good geometry (rms bond distances = 0.007 Å, rms bond angles = 1.32°) and includes residues 55−152 of Grb2, the ligand, and 70 H_2O molecules.

The experimental X-ray data and the refined coordinates of the Grb2-SH2 complexes with **1** and **21** have been deposited in the Protein Data Bank, Biology Department, Brookhaven National Laboratories, Upton, NY 11973, under the file names 1bmb, r1bmbsf, 1bm2, and r1bm2sf (coordinate entry and structure factor entry, complex with **1** and **21**, respectively).

Molecular Modeling. The amino acid sequences Lys-Pro-Phe and Glu-Phe were removed from the ligand in the X-ray structure and Pro-Cys-S-S-*N*-acetyl-Pro was added to the fragment of the remaining ligand (Y*VNV). All free valences were filled with protons. All water molecules were removed, and we selected one of the two alternative side-chain conformations of the disordered Leu97 and Val99. Inter- and intramolecular distance range constraints were defined based on the described[6,13] interactions of Asn and Y* with Grb2-SH2 and the presence of a type-1 β-turn within the ligand. A limited energy minimization using the Tripos force field in Sybyl version 6.5[28] with no electrostatics component was performed for the entire complex to relieve the most severe steric interactions. Gasteiger−Marsili[28] net atomic charges were calculated (with a formal charge of −2/3 assigned to each of the three monovalent oxygen atoms of the fully deprotonated phosphate group). All atoms of the protein were fixed for the remainder of the calculations, and a molecular mechanics optimization including electrostatics (with a distance-dependent dielectric constant of 1*r and an infinite cutoff for nonbonded interactions) was performed with the ligand allowed to relax under the influence of the range constraints. The energy-minimized model was submitted to a molecular dynamics (NTV-ensemble) simulation at 900 K for 50 000 fs with a 1-fs step size. Structures taken at 500-fs intervals of the molecular dynamics calculation (total of 100 conformers) were extracted from the dynamics trajectory and were optimized with the same fixed atom set and range constraints as used for the first geometric relaxation of the docked ligand, until the rms gradient was less than 0.005 kcal/mol Å. Clustering of these 100 low-energy conformers was performed manually by analysis of the hydrogen bonding pattern of each conformer.

NMR Spectroscopy. The compounds (∼3.0 mg) were dissolved in 0.5 mL of 90% H_2O/10% D_2O (CIL, 100%). NMR spectra were recorded on a Bruker AMX-500 NMR spectrometer. Data were processed and analyzed using FELIX (MSI). Chemical shifts are reported relative to the residual proton resonance of H_2O at 4.84 ppm at 293 K. Phase-sensitive DQF-COSY[30] (double-quantum-filtered correlated spectroscopy) and rotating-frame Overhauser effect spectroscopy (ROESY[31]) spectra were recorded using time proportional phase incrementation (TPPI). Two-dimensional spectra were collected with 4096 complex points in the t_2 dimension, 512 increments in the t_1 dimension, and postacquisition delays of 1.5 s. The spectral width in each dimension was 5555.56 Hz. The DQF-COSY[30] spectra and ROESY[31,32] spectra for **2, 25, 26, 27,** and **22** were collected with 8 and 32 acquisitions per t_1 increment, respectively. A spin−lock time of 250 ms was used for the ROESY experiments. Apodization of DQF-COSY data was accomplished by the application of a $\pi/2$ shifted squared-sine bell multiplication in the t_2 dimension and a nonshifted squared-sine bell multiplication in the t_1 dimension. ROESY spectra were processed using a $\pi/2$ shifted squared-sine bell multiplication in both time dimensions.

Chemistry. Solid-phase peptide synthesis was carried out manually (**3, 6**−**8**) or automated (**1, 2, 24**) on an Applied Biosystems peptide synthesizer ABI 433A using Fmoc strategies with the acid-labile *p*-(benzyloxy)benzyl alcohol resin (Wang resin, ∼0.96 mmol/g, 1% cross-linked divinylbenzene styrene copolymer (100−200 mesh); Bachem). DMF was stored over molecular sieves and purged with dry nitrogen. The amino acid derivatives were purchased from Bachem Inc., Aziridine was purchased from Marshallton Labs. All other chemicals were of puriss p.a. quality and used without further purifica-

tion. The attachment of the first amino acid (Fmoc-Pro) was accomplished by using 2,6-dichlorobenzoyl chloride in DMF.[33] Substitution level was determined by Fmoc titration: 0.69 mmol/g. *N*-Acetyl-*S*-(2-aminoethyl)cysteine (*N*-α-acetylthialysine) was synthesized starting from *N*-acetylcysteine and aziridine.[34] Analytical RP-HPLC was performed using a Vydac RP-C18 column together with a binary mobile phase system consisting of 0.1%TFA (v/v) in H_2O (A) and 0.1%TFA (v/v) in CH_3CN (B). Method A: A linear gradient of 10−70% B over 30 min. Method B: A linear gradient of 5−100% B over 30 min. Both methods at a flow rate of 0.8 mL/min and monitoring at 230, 254, and 280 nm. Preparative RP-HPLC was done on a Waters Delta Prep 4000 using two Delta Pack C18 columns (100 Å, 25 × 100 mm) fitted in a radial compression housing. Purification was achieved by a linear gradient from 10% to 60% B in 30 min at a flow rate of 20 mL/min. ^{1}H NMR were recorded at 300 MHz; chemical shifts are reported in ppm. Mass spectral data were obtained by electrospray mass spectroscopy. Optical rotations were measured using a Perkin-Elmer 141 polarimeter. Amino acid analyses (AAA) were performed at Novartis Basel. Amino acids are of L-configuration unless otherwise indicated. Analytical thin-layer chromatography was performed on silica gel 60 F_{254} glass plates (HPTLC, Merck). Preparative column chromatography was performed on silica gel (230−400 mesh, 60 Å) under pressure (∼0.2 mPa). Representative methods for all compounds synthesized according to Scheme 1 are described.

Peptides 1, 2, and 24: All Fmoc-AAs (5 equiv) were single-coupled using *O*-(benzotriazol-1-yl)-*N*,*N*,*N*′,*N*′-tetramethyluronium hexafluorophosphate (HBTU)/HOBt or HBTU/HOAt activation except the amino acid N-terminal to the phosphotyrosine residue was double-coupled. The phosphotyrosine residue was incorporated as a monomer using Fmoc-Tyr[OPO-$(NMe_2)_2$]-OH[18] which was single-coupled (HBTU/HOAt). Side-chain-protecting groups used included Fmoc-Asn(Trt), Fmoc-Cys(Trt), Fmoc-Glu(OtBu), Fmoc-Gln(Trt), and Fmoc-Lys(Boc).

Peptide Purification. After the synthesis was complete the peptide-resin was washed with DCM and dried in vacuo (1−12 h). The peptide was simultaneously deprotected and cleaved from the resin by treatment with a TFA-based cleavage mixture (5−10 mL, 0 °C, 90 min) of either cocktail A (TFA/H_2O/EDT, 95:2.5:2.5) or cocktail B (TFA/phenol/H_2O/EDT/thioanisole, 82.5:5:5:5:2.5), depending on AA and protecting group content. The resin was removed from the peptide solution by filtration and washed once with CH_2Cl_2. The crude peptide was precipitated from the filtrate using anhydrous Et_2O (30−45 mL) and centrifuged. The Et_2O was decanted, and the peptide pellet was, in the same manner, washed with Et_2O (1−2×) and dried in vacuo. The crude peptide was purfied by preparative RP-HPLC. Fractions found to be >95% pure were pooled and lyophilized affording a white powder.

Cyclization. The procedure described by Tam et al. was modified.[35] Briefly, the linear precursor of **2** was dissolved in a minimum volume of 5% AcOH/H_2O. The pH was adjusted to pH 6 using $(NH_4)_2CO_3$. After the addition of 20% v/v DMSO, 10 equiv of Ekathiox resin (Sigma) was added, and the heterogeneous mixture stirred for 4 h. The reaction mixture was filtered through a glass fiber filter to remove the resin and directly injected onto the preparative RP-HPLC. Yield: 80%.

***N*-Fmoc-*O*-[(2,6-dichlorophenyl)methyl]-tyrosyl-valyl-asparagyl-valyl-prolyl-Wang Resin (3).** The Fmoc-protected dipeptide *N*-[(9-fluorenylmethyl)carbonyl]-asparagyl-valine was prepared as follows: A −30 °C solution of *N*-[(9-fluorenylmethyl)carbonyl]-asparagine (10 g, 28.2 mmol) and HOBt (4.58 g, 33.9 mmol) in DMF (60 mL) was treated with DIC (4.42 mL, 28.2 mmol). After the mixture stirred for 90 min while warming up to 5 °C, valine *tert*-butyl ester hydrochloride (8.8 g, 41.9 mmol) and DIEA (10 mL, 57.4 mmol) were added. After 3 h at room temperature, the solvent was removed in vacuo and the residue distributed between EtOAc containing 25% 2-propanol and 1 N HCl. The organic layer was washed with saturated $NaHCO_3$ solution and brine and dried over $MgSO_4$. Removal of the solvent afforded a solid which was then washed with *i*-PrOH and dried in vacuo. The white solid (12 g) was dissolved in TFA/H_2O (12/ 3 mL). After 20 min the solvents were removed in vacuo and fresh TFA/H_2O (12/3 mL) was added. Evaporation of the solvents in vacuo and trituration with THF afforded a white solid (9.74 g, 76% based on Fmoc-Asn) (TLC (CH_2Cl_2/CH_3OH/HOAc, 90/8/2)). ^{1}H NMR (DMSO-d_6) δ: 0.86 (d, J = 7 Hz, 6H); 2.08 (h, J = 7 Hz, 1 H); 2.41/2.53 (AB part of ABX, J = 12, 8, 5 Hz, 2H); 4.15 (dd, J = 8, 5 Hz, 1 H), 4.23 (bs, 3H); 4.43 (m, 1H); 6.95 (s, 1H); 7.30, 7.40 (2t, J = 7 Hz, 4H); 7.55 (d, J = 8 Hz, 1H); 7.70, 7.90 (2d, J = 7 Hz, 4H). Fmoc-Pro-Wang resin (5.0 g, 3.45 mmol) was deprotected with 20% piperidine in DMF (2 × 50 mL, first 1 min, then 20 min) and rinsed with DMF (5 × 50 mL, 5 min each). Fmoc-protected Asn-Val, Val, and *O*-2,6-dichlorobenzyl-Tyr were condensed in sequence using a 2-fold excess each of acid, DIC, and HOBt in DMF (50 mL). The extent of coupling was judged by ninhydrin test.[36] The reaction was usually complete after 5 h; only coupling of Fmoc-Val required coupling overnight. DMF was used in the washing cycles (5 × 50 mL, 5 min each), and 20% piperidine in DMF (2 × 50 mL) was used for Fmoc deprotection (first 1 min, then 20 min). After the final coupling step, the resin was washed with DMF (3 × 50 mL, 5 min each) and CH_2Cl_2 (3 × 50 mL, 5 min each) and dried in vacuo. Yield of the resin-bound Boc-protected peptide: 6.71 g of **3** (faint yellow resin, 93% based on Fmoc-P loading).

(*S*)-*N*-Acetyl-*S*-[2-(*tert*-butoxycarbonyl)aminoethyl]-cysteine (5). A stirred solution of *N*-acetyl-*S*-(2-aminoethyl)-cysteine[34] (800 mg, 3.88 mmol) in H_2O (10 mL) was treated with aqueous $NaHCO_3$ (411 mg, 3.88 mmol) and a solution of di-*tert*-butyl dicarbonate (850 mg, 3.88 mmol) in THF (10 mL). The reaction was stirred for 3 h, diluted with H_2O, and extracted with Et_2O. The aqueous layer was acidified (pH ∼2) with diluted HCl and extracted with EtOAc. The organic layer was dried over $MgSO_4$ and the solvent removed in vacuo. Yield: 1.1 g of **5** as a colorless oil (93%). $[\alpha]_D^{25} = -7.3°$ (c = 2 in EtOAc) (CH_2Cl_2/CH_3OH/HOAc, 90/8/2). ^{1}H NMR (DMSO-d_6) δ: 1.18 (s, 9H); 1.87 (s, 3H); 2.55 (t, J = 6 Hz, 2H); 2.73, 2.90 (AB part of ABX, J = 12, 8, 5 Hz, 2H), 3.08 (q, J = 6 Hz, 2H); 4.35 (m, 1H); 6.90 (m, 1H); 8.10 (d, J = 7 Hz). **4** was prepared the same way. $[\alpha]_D^{25} = +10.0°$ (c = 2 in EtOAc).

***N*-(*tert*-Butoxycarbonyl)-*N*-*a*-acetyl-D-thialysyl-*O*-[(2,6-dichlorophenyl)methyl]-tyrosyl-valyl-asparagyl-valyl-prolyl-Wang Resin (7).** Resin 3 (1.0 g, 0.480 mmol) was deprotected with 20% piperidine in DMF (2 × 10 mL, first 1 min, then 20 min) and rinsed with DMF (5 × 10 mL, 5 min each). **5** was condensed using a 2-fold excess of each acid, DIC, and HOBt in DMF (10 mL). After 3 h (ninhydrin test), the resin was washed with DMF (3 × 10 mL, 5 min each), HOAc (2 × 10 mL, 5 min each), and CH_2Cl_2 (3 × 10 mL, 5 min each), and dried in vacuo. Yield of the resin bound Boc-protected peptide: 1.03 g of **7** (pale yellow resin, 100% based on Fmoc-P loading). **6** was prepared the same way.

5-[*N*-(*tert*-Butoxycarbonyl)amino]-(pentyloxycarbonyl)-*O*-[(2,6-dichlorophenyl)methyl]-tyrosyl-valyl-asparagyl-valyl-prolyl-Wang Resin (8). An ice-cold solution of pyridine (117 μL, 1.46 mmol) in dry CH_2Cl_2 (5 mL) was treated with phosgene (0.746 mL, 1.93 M solution in toluene, 1.44 mmol) and added dropwise to a solution of 5-[*N*-(*tert*)-butoxycarbonyl)-amino]pentanol (293 mg, 1.44 mmol) in CH_2Cl_2 (5 mL). After stirring for 30 min at 0 °C, the clear reaction mixture was added to a suspension of Fmoc-deprotected **3** (1.0 g, 0.480 mmol) in DMF (3 mL). After 12 h at room temperature, the resin was washed with DMF (3 × 10 mL, 5 min each), HOAc (2 × 10 mL, 5 min each), and CH_2Cl_2 (3 × 10 mL, 5 min each), and dried in vacuo. Yield of the resin-bound Boc-protected peptide: 1 g of **8** (faint yellow resin, 100% based on Fmoc-P loading).

***N*-*a*-Acetyl-D-thialysyl-*O*-[(2,6-dichlorophenyl) methyl]-tyrosyl-valyl-asparagyl-valyl-proline TFA Salt (10).** The resin **7** (1.0 g, 0.466 mmol/g) was stirred with a solution of 2% triethylsilane and 8% water in TFA (30 mL) for 2 h and then filtered. The colorless filtrate was evaporated to dryness in vacuo and lyophilized from H_2O/CH_3CN. Yield of **10**: 559

mg (114% based on Fmoc-P loading) as a white fluff. HPLC t_R (method B): 20.2 min. Electrospray MS: 937.3 ([M + H]$^+$, $C_{42}H_{58}Cl_2N_8O_{10}S$, calcd 936.94). **9** was prepared the same way out of **6**: 89%. HPLC t_R (method B): 20.3 min. Electrospray MS: 937.4 ([M + H]$^+$.

5-Amino-(pentyloxycarbonyl)-*O*-[(2,6-dichlorophenyl) methyl]-tyrosyl-valyl-asparagyl-valyl-proline TFA Salt (11). Cleavage from the resin (1.03 g, 0.478 mmol) was done as described for **10**. Yield: 502 mg of **11** (105%) as a white fluff. HPLC t_R (method B): 21.46 min. Electrospray MS: 878.3 ([M + H]$^+$, $C_{41}H_{57}Cl_2N_7O_{10}$, calcd 878.86).

Cyclo-[*N*-*a*-Acetyl-D-thialysyl-*O*-[(2,6-dichlorophenyl)-methyl]-tyrosyl-valyl-asparagyl-valyl-prolyl] (13). A solution of **10** (540 mg, 0.513 mmol) and HOBt (277 mg, 2.05 mmol) in DMF (400 mL) was treated with DPPA (441 μL, 2.05 mmol) and DIEA (1.07 mL, 6.16 mmol). After 48 h, the solvent was removed in vacuo and the residue distributed between EtOAc and 1 N HCl. The organic layer was washed with saturated $NaHCO_3$ solution and brine and dried over $MgSO_4$. The residue, after evaporation, was purified by silica gel column chromatography using CH_2Cl_2/CH_3OH (85:15) as the eluting solvent. Yield of **13**: 315 mg (68%) as a white solid. HPLC t_R (method B): 24.4 min. Electrospray MS: 919.3 ([M + H]$^+$, $C_{42}H_{56}Cl_2N_8O_9S$, calcd 919.93). **12** was prepared the same way out of **9**: 60%. HPLC t_R (method B): 23.9 min. Electrospray MS: 919.3 ([M + H]$^+$.

Cyclo-[5-amino-(pentyloxycarbonyl)-*O*-[(2,6-dichlorophenyl)methyl]-tyrosyl-valyl-asparagyl-valyl-prolyl] (14). Cyclization was done as described for **13**. Yield: 249 mg (62%) of **14** as a white solid. HPLC t_R (method B): 25.6 min. Electrospray MS: 860.4 ([M + H]$^+$, $C_{41}H_{55}Cl_2N_7O_9$, calcd 860.84.

Cyclo-[*N*-α-acetyl-D-thialysyl-tyrosyl-valyl-aspargyl-valyl-prolyl] (16). A solution of 10% Pd/C (315 mg) in EtOH containing 10% formic acid (100 mL) was added to the protected cyclic peptide **13** (315 mg, 0.342 mmol) in a small volume of EtOH. The mixture was left to shake for 16 h under 50 psi of H_2 and 70 °C. After cooling to room temperature, the mixture was filtered through Celite and the filtrate rotary evaporated to dryness. The residue was purified by silica gel column chromatography with elution by CH_2Cl_2/CH_3OH (85:15) and lyophilized from CH_3CN/H_2O. Yield **16**: 150 mg (58%) as a white flocculant solid. HPLC t_R (method B): 16.15 min. Electrospray MS: 761.3 ([M + H]$^+$, $C_{35}H_{52}N_8O_9S$, calcd 760.91). **15**: 155 mg (67%). HPLC t_R (method B): 15.51 min. Electrospray MS: 761.4 ([M + H]$^+$.

Cyclo-[5-amino-(pentyloxycarbonyl)-tyrosyl-valyl-asparagyl-valyl-prolyl] (17). Catalytic hydrogenation was done at room temperature in EtOH using 10% Pd/C. Yield: **17** (100%) as a flocculant solid (lyophilized from CH_3CN/H_2O). HPLC t_R (method B): 17.37 min. Electrospray MS: 702.4 ([M + H]$^+$, $C_{34}H_{51}N_7O_9$, calcd 701.83).

Cyclo-[*N*-*a*-acetyl-D-thialysyl-*O*-[bis(dimethylamino)-phosphotyrosyl]-valyl-asparagyl-valyl-prolyl] (19). 16 (150 mg, 0.197 mmol) was dissolved in dry CH_2Cl_2 (5 mL) and a minimum amount of dry DMF. While stirring in an ice bath, the solution was treated with DMAP (96 mg, 0.788 mmol), DBU (87 μL, 0.591 mmol), and tetramethylphosphorodiamidic chloride (129 μL, 0.788 mmol). After stirring for 1 h at 0 °C and 1 h at room temperature, the solvents were evaporated in vacuo; the residue was dissolved in H_2O, treated with 2.36 mL of 1 N NaOH, and filtered over Amberlite IR-120 (plus) ion-exchange resin (~10 mL). The filtrate was neutralized with 28% NH_4OH and rotary evaporated to dryness. The residue was purified by silica gel column chromatography with elution by CH_2Cl_2/CH_3OH (85:15) and lyophilized from CH_3CN/H_2O. Yield of **19**: 53%. HPLC t_R (method B): 16.3 min. **18**: 83 mg (47%) as a flocculant solid. HPLC t_R (method B): 15.7 min. Electrospray MS: 895.4 ([M + H]$^+$, $C_{39}H_{63}N_{10}O_{10}PS$, calcd 895.04).

Cyclo-[5-amino-(pentyloxycarbonyl)-*O*-[bis(dibenzyl)-phosphotyrosyl]-valyl-asparagyl-valyl-prolyl] (20). An ice-cold solution of **17** (70 mg, 010 mmol) and tetrazole (35 mg, 0.50 mmol) in dry THF (5 mL) and a minimum amount of DMF (to achieve complete solution) was treated with dibenzyl isopropylphosphoramidite (101 μL, 0.30 mmol). After stirring for 2 h at room temperature the reaction was cooled in an ice bath and again treated with *tert*-butyl hydroperoxide (101 μL, 5 N in decane) and stirred for 2 h. The reaction mixture was distributed between EtOAc and 1 N HCl. The organic layer was washed with saturated $NaHCO_3$ solution and brine and dried over $MgSO_4$. The residue, after evaporation, was purified by silica gel column chromatography using CH_2Cl_2/CH_3OH (90:10) as the eluting solvent. Yield: 68 mg of **20** (70%) as a white solid. HPLC t_R (method B): 24.47 min. Electrospray MS: 962.3 ([M + H]$^+$, $C_{48}H_{64}N_7O_{12}P$, calcd 962.06).

Cyclo-[*N*-α-Acetyl-D-thialysyl-*O*-phosphotyrosyl-valyl-asparagyl-valyl-prolyl] (22). A solution of **19** (60 mg, 0.067 mmol) in 1 N HCl (10 mL) was stirred for 16 h. The solvent was evaporated and purified by RP-HPLC. Yield of **22**: 61%. HPLC t_R (method A): 13.37 min. Electrospray MS: 841.4 ([M + H]$^+$, $C_{35}H_{53}N_8O_{12}PS$, calcd 840.90). **21**: 30 mg (53%) as a flocculant solid. HPLC t_R (method A): 12.66 min. Electrospray MS: 841.4 ([M + H]$^+$, $C_{35}H_{53}N_8O_{12}PS$, calcd 840.90).

Cyclo-[5-amino-(pentyloxycarbonyl)-*O*-phosphotyrosyl-valyl-asparagyl-valyl-prolyl] (23). Catalytic hydrogenation as described for **17** yielded **23**: 88%. HPLC t_R (method A): 14.96 min. Electrospray MS: 782.3 ([M + H]$^+$, $C_{34}H_{52}N_7O_{12}P$, calcd 781.81).

Acknowledgment. The authors are grateful to M. Zvelebil, S. Vijayakumar, and N. Nirmala for helpful discussions and to H. Radzyner-Vyplel for his support in generating Figures 1 and 2. We thank P. Pattison, K. Knudsen, and collaborators at BM01a of the ESRF, Grenoble, for support in X-ray data collection.

Supporting Information Available: Analytical data for compounds **1**−**33**. This material is available free of charge via the Internet at http://pubs.acs.org.

References

(1) Preliminary report: Ettmayer, P.; France, D.; Gounarides, J.; Jarosinski, M.; Martin, M.-S.; Rondeau, J.-M.; Sabio, M.; Weidmann, B.; Zurini, M.; Bair, K. W. Structural/conformational requirements for high affinity binding to the SH2 domain of Grb2. *Proc. Am. Assoc. Cancer Res.* **1998**, *39*, 176 (Abstract #1203).

(2) Mayer, B. J.; Gupta, R. Functions of SH2 and SH3 domains. *Curr. Top. Microbiol. Immunol.* **1998**, *228*, 1−22. Chook, Y. M.; Gish, G. D.; Kay, C. M.; Pai, E. F.; Pawson, T. The Grb2-mSos1 Complex Binds Phosphopeptides with Higher Affinity than Grb2. *J. Biol. Chem.* **1996**, *271*, 30472−30478. Clark, J. W.; Santos-Moore, A.; Stevenson, L. E.; Frackelton, A. R., Jr. Effects of tyrosine kinase inhibitors on the proliferation of human breast cancer cell lines and proteins important in the ras signaling pathway. *Int. J. Cancer* **1996**, *65*, 186−191. Ricci, A.; Lanfrancone, L.; Chiari, R.; Belardo, G.; Pertica, C.; Natali, P. G.; Pelicci, P. G.; Segatto, O. Analysis of protein−protein interactions involved in the activation of the Shc/Grb-2 pathway by the ErbB-2 kinase. *Oncogene* **1995**, *11*, 1519−1529.

(3) Pendergast, A. M.; Quilliam, L. A.; Cripe, L. D.; Bassing, C. H.; Dai, Z.; Li, N.; Batzer, A.; Rabun, K. M.; Der, C. J.; Schlessinger, J. BCR-ABL-induced oncogenesis is mediated by direct interaction with the SH2 domain of the GRB-2 adaptor protein. *Cell* **1993**, *75*, 175−185. Tari, A. M.; Arlinghaus, R.; Lopez-Berestein, G. Inhibition of Grb2 and Crkl proteins results in growth inhibition of Philadelphia chromosome positive leukemic cells. *Biochem. Biophys. Res. Commun.* **1997**, *235*, 383−388.

(4) Ward, C. W.; Gough, K. H.; Rashke, M.; Wan, S. S.; Tribbick, G.; Wang, J.-X. Systematic mapping of potential binding sites for Shc and Grb2 SH2 domains on insulin receptor substrate-1 and the receptors for insulin, epidermal growth factor, platelet-derived growth factor, and fibroblast growth factor. *J. Biol. Chem.* **1996**, *271*, 5603−5609.

(5) Jarosinski, M. Unpublished results.

(6) Rahuel, J.; Gay, B.; Erdmann, D.; Strauss, A.; García-Echeverria, C.; Furet, P.; Caravatti, G.; Fretz, H.; Schoepfer, J.; Grütter, M. G. Structural basis for specificity of GRB2−SH2 revealed by a novel ligand binding mode. *Nature Struct. Biol.* **1996**, *3*, 586.

(7) Ogura, K.; Tsuchiya, S.; Terasawa, H.; Yuzawa, S.; Hatanaka, H.; Mandiyan, V.; Schlessinger, J.; Inagaki, F. Conformation of an Shc-derived phosphotyrosine-containing peptide complexed with the Grb2 SH2 domain. *J. Biomol. NMR* **1997**, *10*, 273−278.

(8) Kuriyan, J.; Cowburn, D. *Annu. Rev. Biol. Biophys. Biomol. Struct.* **1997**, *26*, 259−288. For a detailed list of papers reporting about X-ray and NMR structures of ligated SH2 domains, see also ref 20 in ref 21.
(9) Marengere, L. E.; Songyang, Z.; Gish, G. D.; Schaller, M. D.; Parsons, J. T.; Stern, M. J.; Cantley, L. W.; Pawson, T. SH2 Domain Specificity and Activity Modified by a Single Residue. *Nature* **1994**, *369*, 502−505.
(10) Mueller, K.; Gombert, F. O.; Manning, U.; Grossmuller, F.; Graff, P.; Zaegel, H.; Zuber, J. F.; Freuler, F.; Tschopp, C.; Baumann, G. Rapid identification of phosphopeptide ligands for SH2 domains: Screening of peptide libraries by fluorescence-activated bead sorting. *J. Biol. Chem.* **1996**, *271*, 16500−16505. Gram, H.; Schmitz, R.; Zuber, J. F.; Baumann, G. Identification of phosphopeptide ligands for the Src-homology 2 (SH2) domain of Grb2 by phage display. *Eur. J. Biochem.* **1997**, *246*, 633−637.
(11) Ligand residues are numbered relative to the position of the phosphotyrosine which is called Y*.
(12) Gay, B.; Furet, P.; Garcia-Echeverria, C.; Rahuel, J.; Chene, P.; Fretz, H.; Schoepfer, J.; Caravatti, G. Dual Specificity of Src Homology 2 Domains for Phosphotyrosine Peptide Ligands. *Biochemistry* **1997**, *36*, 5712−5718.
(13) Distance range constraints (minimal/maximal distance = 2.3/3.5 Å, constant = 200, power = 2) between the protein (first atom) and the ligand (second atom): LYS109.N/ASN+2.Oδ1; LEU120.O/ASN+2.Nδ2; LYS109.O/ASN+2.Nδ2; PTY0.O/VAL+3.N (ligand-to-ligand); SER90.Oγ/PTY0.OP1; SER88.Oγ/PTY0.OP3;SER88.Oγ/PTY0.OP1;SER96.Oγ/PTY0.OP3;ARG86.NH1/PTY0.OP3; ARG86.NH2/PTY0.OP2; ARG67.NH1/PTY0.OP2.
(14) Zvelebil, M. J. J. M.; Panayotou, G.; Linacre, J.; Waterfield, M. D. Prediction and analysis of SH2 domain − phosphopeptide interactions. *Protein Eng.* **1995**, *8*, 527−533.
(15) Furet, P.; Gay, B.; Garcia-Echeverria, C.; Rahuel, J.; Fretz, H.; Schoepfer, J.; Caravatti, G. Discovery of 3-Aminobenzyloxycarbonyl as an N−Terminal Group Conferring High Affinity to the Minimal Phosphopeptide Sequence Recognized by the Grb2-SH2 Domain. *J. Med. Chem.* **1997**, *40*, 3551−3556.
(16) For practical reasons (CPU time), the molecular dynamics simulation was performed only for 50 000 fs in gas phase. To avoid gas-phase artifacts, the protein atoms were kept fixed.
(17) Asn was used unprotected. No dehydration of the carboxamide was observed during coupling.
(18) Chao, H.-G.; Leiting, B.; Reiss, P. D.; Burkhardt, A. L.; Klimas, C. E.; Bolen, J. B.; Matsueda, G. R. Synthesis and Application of Fmoc-O-[bis(dimethylamino)phosphono]-tyrosine, a Versatile Protected Phosphotyrosine Equivalent. *J. Org. Chem.* **1995**, *60*, 7710−7711.
(19) Wuthrich, K. *NMR of Proteins and Nucleic Acids*; Wiley: New York, 1986.
(20) McNemar, C.; Snow, M. E.; Windsor, W. T.; Prongay, A.; Mui, P.; Zhang, R.; Durkin, J.; Le, H. V.; Weber, P. C. Thermodynamic and structural analysis of phosphotyrosine polypeptide binding to Grb2-SH2. *Biochemistry* **1997**, *36*, 10006−10014.
(21) Garcia-Echeverria, C.; Furet, P.; Gay, B.; Fretz, H.; Rahuel, J.; Schoepfer, J.; Caravatti, G. Potent Antagonists of the SH2 Domain of Grb2: Optimization of the X+1 Position of 3-Amino-Z-Tyr(PO3H2)-X+1-Asn-NH2. *J. Med. Chem.* **1998**, *41*, 1741−1744.
(22) Waksman, G.; Kominos, D.; Robertson, S. C.; Pant, N.; Baltimore, D.; Birge, R. B.; Cowburn, D.; Hanafusa, H.; Mayer, B. J.; Overduin, M.; Resh, M. D.; Rios, C. B.; Silverman, L.; Kuriyan, J. Src-SH2 domain binds phosphopeptides in an extended conformation. *Nature* **1992**, *358*, 646−653.
(23) Smith, D. B.; Johnson, K. S. Single-step purification of polypeptides expressed in *Escherichia coli* as fusions with glutathione S-transferase. *Gene* **1988**, *31*, 67.
(24) Otwinowski, Z.; Minor, W. Processing of X-ray Diffraction Data Collected in Oscillation Mode. *Methods in Enzymology*; Academic Press: New York, 1996; p 276.
(25) Navaza, J. AMoRe: an Automated Package for Molecular Replacement. *Acta Crystallogr.* **1994**, A50, 157−163.
(26) Brünger, A. T. *X-PLOR, Version 3.1: A System for Crystallography and NMR*; Yale University Press: New Haven, CT, 1992.
(27) Engh, R. A.; Huber, R. Accurate Bond and Angle Parameters for X-ray Protein Structure Refinement. *Acta Crystallogr.* **1994**, A47, 392−400.
(28) Sybyl (v. 6.5); Tripos, Inc., 1699 S. Hanley Rd, St. Louis, MO 63144-2913.
(29) Gasteiger, J.; Marsili, M. Iterative partial equalization of orbital electronegativity − a rapid access to atomic charges. *Tetrahedron* **1980**, *36*, 3219−3228.
(30) Rance, M.; Soerensen, O. W.; Bodenhausen, G.; Wagner G.; Ernst, R. R.; Wuethrich, K. Improved spectral resolution in COSY proton NMR spectra of proteins via double quantum filtering. *Biochem. Biophys. Res. Commun.* **1983**, *117*, 479−485.
(31) Bax, A.; Davis, D. G. Practical aspects of two-dimensional transverse NOE spectroscopy. *J. Magn. Reson.* **1985**, *63*, 207−213.
(32) Marion, D.; Wuethrich, K. Application of phase sensitive two-dimensional correlated spectroscopy (COSY) for measurements of proton−proton spin−spin coupling constants in proteins. *Biochem. Biophys. Res. Commun.* **1983**, *113*, 967−974.
(33) Sieber, P. An improved method for anchoring of 9-fluorenylmethoxycarbonyl amino acids to 4-alkoxybenzyl alcohol resins. *Tetrahedron Lett.* **1987**, *28*, 6147−6150.
(34) Hermann, P.; Stalla, K.; Schwimmer, J.; Willhardt, I.; Kutschera, I. Synthesis of some sulfur-containing amino acid analogues. *J. Prakt. Chem.* **1969**, *311*, 1018−1028.
(35) Tam, J. P.; Wu, C. R.; Liu, W.; Zhang, J. W. Disulfide bond formation in peptides by dimethyl sulfoxide. Scope and applications. *J. Am. Chem. Soc.* **1991**, *113*, 6657−6662.
(36) Kaiser, E.; Colescott, R. L.; Bossinger, C. D.; Cook, P. I. Color test for detection of free terminal amino groups in the solid-phase synthesis of peptides. *Anal. Biochem.* **1970**, *34*, 595−598.

JM9811007